

Progress Report February 2022

1. Comparison of Results from MPTS Method, and Established Fitting Methodologies

Before we will present the results from our comparative study, we comment briefly on the various methods involved.

(a) *Multiple-Peak, Tesseral-Spectrum method*

The Multiple-Peak, Tesseral-Spectrum (MPTS) method of Reiter *et al.* (2020) is equally well-suited for the estimation of low-, medium-, and high-degree f- and p-mode parameters and frequency-splitting coefficients. The MPTS method operates directly upon all the modes in a multiplet (n, l) . As a result, $2l + 1$ sets of modal parameters are obtained simultaneously for that multiplet (n, l) . By simply averaging all of the $2l + 1$ frequency estimates within a multiplet, the average frequency for that multiplet is obtained, which is called the “mean-multiplet frequency”. In addition, by fitting an appropriate polynomial to the run of the fitted frequencies versus m , the frequency-splitting coefficients for that multiplet are estimated. Since the errors in the sectoral, tesseral, and zonal power spectra are not normally distributed as they are in the case of the m -averaged spectra (at least for $l \gg 1$), a maximum-likelihood fitting approach is employed in the MPTS method.

The data obtained with the MPTS method which we used in our comparisons, were obtained from the 90d spectra HMI.100430to0728. The table of fitted mode parameters includes a total of 7329 modes in the degree range $0 \leq l \leq 1350$, radial order range $0 \leq n \leq 30$, and frequency range $964.8 \leq \nu < 4600 \mu\text{Hz}$. In the following we will use the term “MPTS” when we are referring to the MPTS method.

(b) *Mean-multiplet technique*

In the mean-multiplet technique of Schou (1992) the Fourier transforms of the gap-filled time series of the spherical harmonic coefficients, which result from the spatial decomposition of the individual Dopplergrams in an observing run, are fit using a maximum likelihood approach, taking into account leakage between the modes (Larson & Schou, 2015). Rather than fitting, however, for the individual $2l + 1$ mode frequencies within a multiplet (n, l) , this technique includes a fitting algorithm that yields the mean-multiplet frequency $\nu_{n,l}$ and the set of frequency-splitting coefficients $a_k^{(n,l)}$ for each multiplet directly, assuming that the line width and the amplitude of the $2l + 1$ modes are independent of the azimuthal order m . Initially, the algorithm fits for a total of 6 frequency-splitting coefficients, then for 18 and 36 once the 6-term fits have converged. Leaks from multiplets other than (n, l) are taken into account. The asymmetry of the line profiles is taken into account by using an asymmetrical profile that is derived by a generalization of the profile of Nigam & Kosovichev (1998). This way undesirable properties of the profile of Nigam & Kosovichev (1998) are avoided, viz. its invalidity far from the mode frequency and the non-boundedness of its integral over all frequencies (Larson & Schou, 2015).

The data obtained with the mean-multiplet technique which we used in our comparisons, viz. `hmi.V_sht_modes_asym.20100430_000000_TAI.0.300.691200.m10qr.6328.36`, were downloaded from `jsoc.stanford.edu`. For the details of their generation we refer to Larson & Schou (2015). In the following we will use the term “JS” when we are referring to the mean-multiplet technique.

(c) *Fitting methodology of Korzennik*

The fitting methodology of Korzennik *et al.* (2004) is applicable to high-degree modes with degrees in the range from $l \gtrsim 100$ (p-modes) to $l \gtrsim 200$ (f-modes). Its basic idea consists of correcting for the bias introduced when fitting a ridge of power at high degrees. For this purpose, a detailed model of the underlying modes that contribute to the distribution of power in a ridge was developed to generate synthetic ridges, which are then fitted using the same methodology employed to fit the observations. Hence, the results of fitting these synthetic data allow the user to derive a measure of the bias between the ridge properties and those of the underlying targeted mode used in the modeling. By means of this measure the results from fitting an observed ridge can be corrected to derive the unbiased properties of the underlying targeted mode.

The data obtained with the fitting methodology of Korzennik which we used in our comparisons, viz. `multiplets-hmi-2010.dat`, were downloaded from `lweb.cfa.harvard.edu/~sylvain/research/tables/HiL/HMI/2010/`. For the details of their generation we refer to Korzennik *et al.* (2013). In the following we will use the term “SK” when we are referring to the fitting methodology of Korzennik.

(d) *Fitting methodology of the Birmingham Solar Oscillations Network group*

The fitting methodology of the Birmingham Solar Oscillations Network (BiSON) group is applicable to low-degree modes with degrees in the range from $0 \leq l \leq 3$, and is described in detail in Broomhall *et al.*, MNRAS 396 (2009), in Davies *et al.*, MNRAS 439 (2014), and in Hale *et al.*, Sol. Phys. 291 (2016).

The BiSON network comprises six semi-automated solar observing stations that are dedicated to the collection of low-degree (Sun-as-a-star) helioseismic data. The stations are situated at various sites around the world in order to provide as continuous observations as possible. At each of the six stations, a resonance scattering spectrometer (RSS) is used to measure the Doppler velocity shift of the 770-nm D1 potassium absorption line by comparing the Doppler shifted potassium absorption line to a reference line in the laboratory frame. These shifts are measured as variations in resonant scattered intensity which are calibrated into radial velocities each day for each of the six stations. Using these data, a time series is built based on a routine that attempts to maximize the signal-to-noise ratio in the low-frequency region (0.8-1.3 mHz). This time series is then converted to the frequency domain using a fast Fourier transform (FFT) to generate the frequency power spectrum. Finally, a maximum-likelihood approach is employed to fit an asymmetric Lorentzian profile to the peaks in the frequency power spectrum, the parameters being frequency, amplitude, width, rotational splitting and fractional asymmetry.

The data obtained with the fitting methodology of the Birmingham Solar Oscillations Network group which we used in our comparisons, viz. `broomhall2009.txt`, were downloaded from `bison.ph.bham.ac.uk/opendata`. In the following we will use the term “BR” when we are referring to the fitting methodology of the Birmingham Solar Oscillations Network group.

Before we will present the results from our comparative study, we list in Table 1 the starting date, duration, average of the MgII core-to-wing ratio (also known as the MgII index), and average of the 10.7-cm flux for the observations analyzed with the MPTS, JS, SK, and BR fitting methodologies.

It is clear from Table 1 that the individual observing runs have been influenced by the differing

	starting date	duration	MgII index	10.7-cm flux
MPTS	2010.04.30	90d	0.265905	77.207
JS	2010.04.30	360d	0.266969	80.916
SK	2010.05.07	67d	0.265654	74.988
BR	1985.04.04	8640d	0.265000	64.000

Table 1: Starting date, duration, average of the MgII core-to-wing ratio (also known as the MgII index), and average of the 10.7-cm flux for the observations analyzed with the MPTS, JS, SK, and BR fitting methodologies. The starting date is given in the form yyyy.mm.dd. The duration is measured in days, and the 10.7-cm flux is measured in units of $10^{-22}\text{Wm}^{-2}\text{Hz}^{-1}$. The BR observations are pertinent to the canonical “quiet-Sun” level of the radio flux, which, from historical observations of the index, is set at $64 \times 10^{-22}\text{Wm}^{-2}\text{Hz}^{-1}$.

average levels of solar activity during those runs. Thus, it will be mandatory to correct the JS, SK, and BR frequencies according to the level of the MPTS observing run before comparing them with the MPTS frequencies. Similar correction procedures will need to be applied for the comparisons of both the SK and BR frequencies with the JS frequencies. We explicitly point out that in this month’s report we have refrained from such corrections. We plan to do so for our next monthly report.

In Table 2 we show the results of our comparison of the uncorrected JS, SK, and BR frequencies with the MPTS frequencies, and the uncorrected SK and BR frequencies with the uncorrected JS frequencies.

difference	n_d	raw				normalized		
		ave	std	t	p	ave	std	$n_{\pm 3\sigma}$
JS–MPTS	2030	+0.008	0.143	2.487	0.006	+0.270	1.600	148
SK–MPTS	4690	−1.289	1.233	71.621	≈ 0	−8.752	6.769	3617
BR–MPTS	76	−0.003	0.320	0.838	0.202	−0.176	1.113	1
SK–JS	540	−0.046	1.662	0.639	0.262	−0.641	4.225	168
BR–JS	49	−0.027	0.119	1.588	0.059	−0.807	1.407	4

Table 2: Comparison of the MPTS method with the JS, SK, and BR methods, the SK method with the JS method, and the BR method with the JS method in terms of raw (uncorrected) and normalized frequency differences. The differences are in the sense as indicated in the first column. The normalization was carried out by dividing the raw differences by the formal error of each difference. For both the raw and the normalized frequency differences the average and the standard deviation are listed in the columns labeled ave and std, respectively. Using Student’s t-test, each mean raw frequency difference was tested for a significant deviation from zero. The t -value and the probability that the sample difference occurred by chance are listed in the columns labeled t and p , respectively. In the column labeled n_d the sample sizes are given, while in the column labeled $n_{\pm 3\sigma}$ the number of cases are listed for which the normalized frequency difference exceeds 3σ in absolute magnitude. The raw frequency differences are measured in μHz .

In Figure 1 we show the differences of the uncorrected JS frequencies and the MPTS frequencies as functions of frequency. Since the average level of activity during the 360-day JS time series was higher than the 90-day average level, we would expect that the average difference $\nu_{\text{JS}} - \nu_{\text{MPTS}}$ is positive, and according to Table 2 it is.

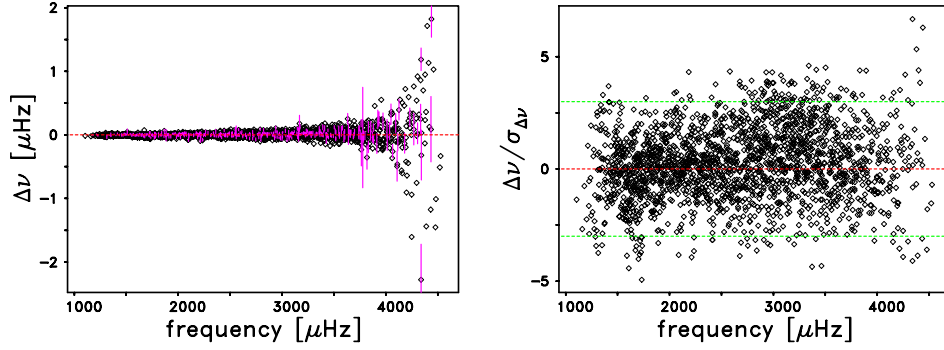


Figure 1: (Left panel) Raw (uncorrected) differences, $\Delta\nu = \nu_{\text{JS}} - \nu_{\text{MPTS}}$, as functions of frequency. For every 5th difference the error bar is shown in magenta, and the dashed red line is for a difference of zero. The error bars are the square root of the sum of the squares of the uncertainties of the two sets of frequencies. (Right panel) Normalized differences, $\Delta\nu/\sigma_{\Delta\nu}$, of the frequencies, as function of frequency. The normalization was carried out by dividing the raw differences by the formal error of each difference. The dashed red line is for a difference of zero, while the dashed green lines show the $\pm 3\sigma$ values.

In Figure 2 we show the differences of the uncorrected SK frequencies and the MPTS frequencies as functions of frequency. Since the average level of activity during the 67-day SK time series was lower than the 90-day average level, we would expect that the average difference $\nu_{\text{SK}} - \nu_{\text{MPTS}}$ is negative, and according to Table 2 it is. Also, a clear downward trend with frequency is to be seen.

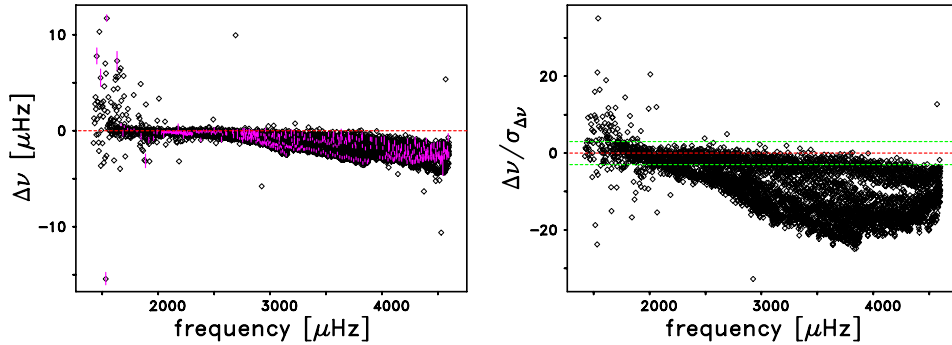


Figure 2: (Left panel) Raw (uncorrected) differences, $\Delta\nu = \nu_{\text{SK}} - \nu_{\text{MPTS}}$, as functions of frequency. For every 10th difference the error bar is shown in magenta, and the dashed red line is for a difference of zero. The error bars are the square root of the sum of the squares of the uncertainties of the two sets of frequencies. (Right panel) Normalized differences, $\Delta\nu/\sigma_{\Delta\nu}$, of the frequencies, as function of frequency. The normalization was carried out by dividing the raw differences by the formal error of each difference. The dashed red line is for a difference of zero, while the dashed green lines show the $\pm 3\sigma$ values.

In Figure 3 we show the differences between the uncorrected BR frequencies and the MPTS frequencies as functions of frequency. Since the average level of activity during the 8640-day BR time series was lower than the 90-day average level, we would expect that the average difference $\nu_{\text{BR}} - \nu_{\text{MPTS}}$ is negative, and according to Table 2 it is but only a tiny amount of 3 nHz. Also, there seems to be no systematic trend of the differences with frequency.

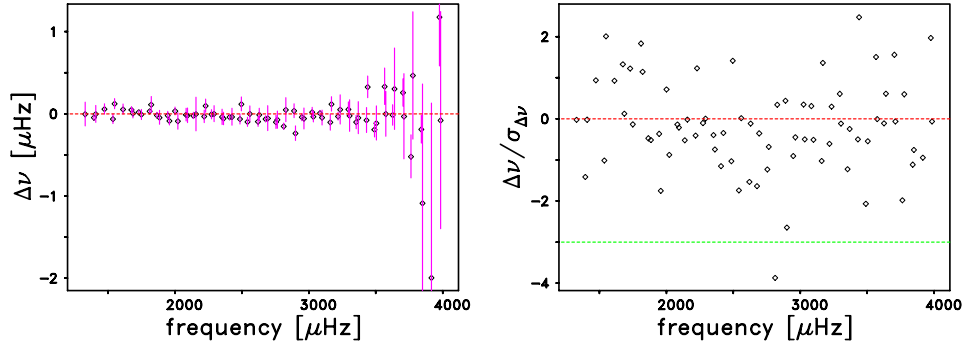


Figure 3: (Left panel) Raw (uncorrected) differences, $\Delta\nu = \nu_{\text{BR}} - \nu_{\text{MPTS}}$, as functions of frequency. For every difference the error bar is shown in magenta, and the dashed red line is for a difference of zero. The error bars are the square root of the sum of the squares of the uncertainties of the two sets of frequencies. (Right panel) Normalized differences, $\Delta\nu/\sigma_{\Delta\nu}$, of the frequencies, as function of frequency. The normalization was carried out by dividing the raw differences by the formal error of each difference. The dashed red line is for a difference of zero, while the dashed green lines show the $\pm 3\sigma$ values.

In Figure 4 we show the differences of the uncorrected SK and JS frequencies as functions of frequency. Since the average level of activity during the 67-day SK time series was lower than the 360-day average level of the JS time series, we would expect that the average difference $\nu_{\text{SK}} - \nu_{\text{JS}}$ is negative, and according to Table 2 it is. Also, a slight downward trend of the differences with frequency can be seen.

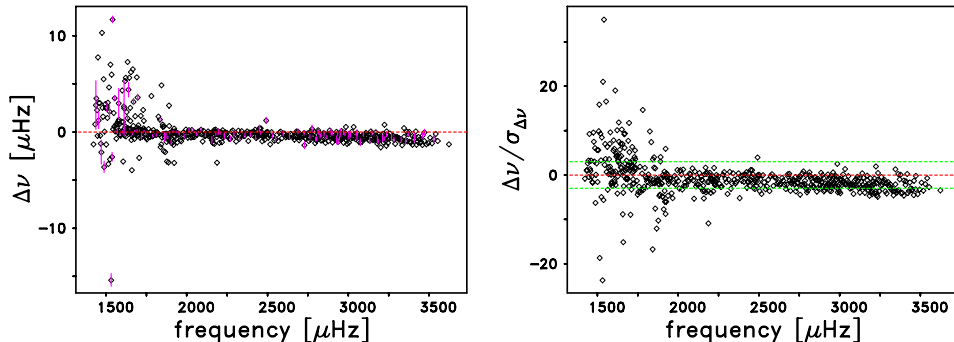


Figure 4: (Left panel) Raw (uncorrected) differences, $\Delta\nu = \nu_{\text{SK}} - \nu_{\text{JS}}$, as functions of frequency. For every 5th difference the error bar is shown in magenta, and the dashed red line is for a difference of zero. The error bars are the square root of the sum of the squares of the uncertainties of the two sets of frequencies. (Right panel) Normalized differences, $\Delta\nu/\sigma_{\Delta\nu}$, of the frequencies, as function of frequency. The normalization was carried out by dividing the raw differences by the formal error of each difference. The dashed red line is for a difference of zero, while the dashed green lines show the $\pm 3\sigma$ values.

Finally, in Figure 5 we show the differences of the uncorrected BR and JS frequencies as functions of frequency. Since the average level of activity during the 8640-day BR time series was lower than the 360-day average level of the JS time series, we would expect that the average difference $\nu_{\text{BR}} - \nu_{\text{JS}}$ is negative, and according to Table 2 it is. Also, there seems to be no systematic trend of the differences with frequency.

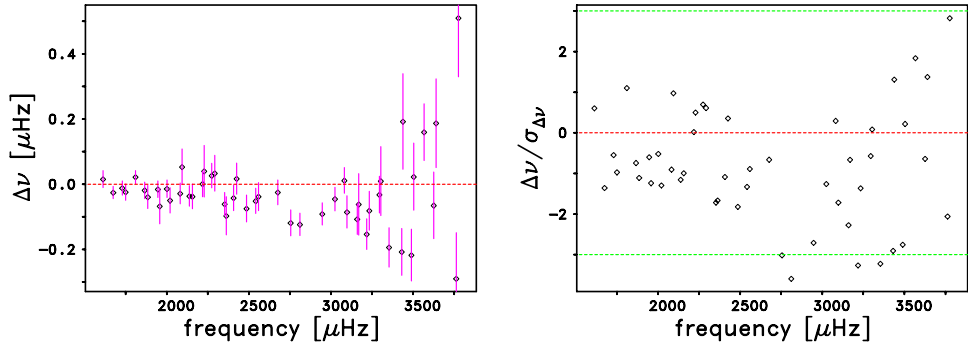


Figure 5: (Left panel) Raw (uncorrected) differences, $\Delta\nu = \nu_{\text{BR}} - \nu_{\text{JS}}$, as functions of frequency. For every difference the error bar is shown in magenta, and the dashed red line is for a difference of zero. The error bars are the square root of the sum of the squares of the uncertainties of the two sets of frequencies. (Right panel) Normalized differences, $\Delta\nu/\sigma_{\Delta\nu}$, of the frequencies, as function of frequency. The normalization was carried out by dividing the raw differences by the formal error of each difference. The dashed red line is for a difference of zero, while the dashed green lines show the $\pm 3\sigma$ values.